IEEE Access
Multidisciplinary ⋮ Rapid Review ⋮ Open Access Journal

Received 27 January 2025, accepted 15 February 2025, date of publication 19 February 2025, date of current version 3 March 2025.

Digital Object Identifier 10.1109/ACCESS.2025.3543703

RESEARCH ARTICLE

Multilevel Inverter Based on a Dual Two-Level Nine-Switch Converter for a Dual Three-Phase or Six-Phase Motor Drive System

V. FERNÃO PIRES[1,2], (Senior Member, IEEE), ARMANDO CORDEIRO[2,3], (Member, IEEE), DANIEL FOITO[1,4], A. J. PIRES[1,4], J. FERNANDO A. SILVA[2,5], (Life Senior Member, IEEE), AND HAO CHEN[6], (Senior Member, IEEE)

[1]Instituto Politécnico de Setúbal, Escola Superior de Tecnologia de Setúbal, Campus do IPS, 2914-508 Setúbal, Portugal
[2]INESC-ID Lisboa, 1000-029 Lisbon, Portugal
[3]ISEL, Lisboa Polytechnic University, 1549-020 Lisbon, Portugal
[4]CTS-UNINOVA and LASI, 2829-516 Costa da Caparica, Portugal
[5]IST, Lisboa University, 1649-004 Lisbon, Portugal
[6]School of Electrical Engineering, China University of Mining and Technology, Xuzhou 221116, China

Corresponding author: A. J. Pires (armando.pires@estsetubal.ips.pt)

This work was supported by the National Funds through the Instituto Politécnico de Setúbal and FCT—Fundação para a Ciência e a Tecnologia under Grant UIDB/50021/2020 and Grant UIDB/00066/2020.

ABSTRACT The nine-switch inverter is considered as a very interesting solution for three-phase dual output applications, such as dual three-phase or six-phase motor drive systems. The main advantage of this approach is a converter topology with a reduced number of power semiconductors. However, the *AC* output voltages are limited to only two levels. This work proposes a new inverter topology for dual three-phase or six-phase motor drive systems with multilevel output characteristics. The proposed topology is based on two isolated inverters, but the number of legs is reduced from six to three. This structure creates a modular multilevel inverter with a high number of voltage levels while using a comparatively smaller number of power semiconductors. A modulation strategy, associated with the proposed topology, is presented to ensure multilevel operation. The proposed topology and modulation strategy will be tested first through a simulation in Matlab/Simulink and then by laboratory tests using an experimental prototype. The obtained results show a good agreement between simulations and experiments, both confirming the theoretical studies.

INDEX TERMS Dual motor, six-phase motor, dual stator, multilevel inverter, nine-switch converter.

I. INTRODUCTION

Nowadays, many applications are using electric motors with dual stator, two motors or even six-phase motors. These applications usually require tight control of the motor speed or the electromagnetic torque. Thus, the use of power electronic converters is essential as motor drivers. There are several voltage source inverter (VSI) topologies that can be used for the drive of the above motors. The choice of the topology depends on several factors. One of the areas on which researchers have concentrated is the design of a VSI trying to decrease the number of passive and active components with the aim of reducing the VSI overall costs.

Several approaches for the design of VSI for motor drives with a reduced number of semiconductor switches have been presented and studied. One of the approaches to reducing the number of power semiconductors considers the elimination of one inverter leg. To compensate for the elimination of this leg, several proposals were made. One proposal uses a DC-link midpoint (B4 inverter) [1], [2]. Another way to compensate for the loss of the inverter leg is to adopt a shared leg (five-leg inverter) [3], [4]. Both solutions reduce the power semiconductor count by two. Another solution to reduce the number of power semiconductors is by using

The associate editor coordinating the review of this manuscript and approving it for publication was Qinfen Lu.

two sets of three-phase interfacing terminals. This topology, called nine-switch converter, saves three power semiconductors [5], [6], [7], [8]. However, this solution is characterized by outputting AC voltages with just two voltage levels. It was suggested to employ topologies that enable the delivery of AC multilevel voltages for motor drives as an alternative to the usage of two-level inverters. The multilevel topologies have a number of benefits over two-level topologies, including AC voltages with lower distortions, an increase in the nominal power of the converter, lower common mode voltages, and lower dv/dt [9]. Given the referred advantages, multilevel topologies have been successfully used in industry. The best known and developed multilevel topologies are the Neutral Point Clamped (NPC), Flying Capacitor (FC) and Cascaded HBridge (CHB) [10], [11], [12]. These topologies have also been applied to motors with open windings. This is the case involving the dual-inverter topology, which has been strongly suggested for use in Electric Aircraft Applications [13]. Various alternative multilevel configurations for these motors have been suggested [14], [15], [16]. Nowadays, these configurations are deemed crucial for managing three-phase motors in electric drives. Nevertheless, they have found applications in other machine types, including dual three-phase or six-phase motors. These motor drives have been used successively in electric vehicles [17], [18], [19], [20], [21]. In this context, many of the multilevel topologies used in multiphase drives are adaptations of the conventional three-phase configurations, featuring additional legs. Hence, the established NPC, FC and CHB VSIs have been extended to be used in drives for six-phase motors [22], [23], [24], [25], [26], [27]. Nevertheless, alternative multilevel configurations specifically designed for six-phase motors have also been put forward. One proposal is derived from three-phase, two-level VSIs. In [28], a particular example of this approach is introduced as the 'hexagram inverter.' However, it requires a relatively high number of DC voltage sources, a high number of switches, and interconnecting inductors. An alternative approach is described in [29]. While it does succeed in reducing the count of DC voltage sources to five, it still demands a substantial number of switches. In [30] and [31], novel topologies are introduced that manage to curtail the number of switches and DC voltage sources. Nevertheless, they still maintain a significant number of switches and the need for three DC voltage sources. In [32], a multilevel configuration aimed at minimizing the requirement of DC voltage sources is presented. However, the number of switches remains comparatively high and requires floating capacitors. Other solutions that enabled the implementation of a multilevel drive for dual or six-phase motors were presented in [33], [34], [35], and [36]. Nevertheless, these solutions still required a high number of switches, DC voltage sources, or even capacitors.

The extension of the nine-switch inverter for a multilevel converter with a reduced number of switches to be used in a dual three-phase or six-phase motor drive system was also proposed. Thus, a dual-output multilevel inverter based on the NPC was proposed [37], [38]. Another extension was for the multilevel nine-switch inverter based on the T-Type structure [39], [40]. Another solution was presented in [41], in which a power circuit derived from the F-type inverter was used to obtain a multilevel converter based on the nine-switch inverter. These very recent multilevel solutions show the interest that has appeared in these kinds of converters. However, taking into consideration the number of voltage levels applied to the motor windings, it is possible to see that the reduction of switch numbers for this kind of applications still remains a concern.

This work is focused on creating a multilevel converter with dual outputs. The planned drive system will prioritize the reduction of the number of power semiconductor components. Consequently, the proposed topology will be based on the dual inverter configuration but with a reduction number of inverter legs. The proposed topology is also characterized by its capability of applying a high number of voltage levels to each motor winding. Besides the theoretical analysis, a mathematical model for this topology will also be presented. Additionally, a sinusoidal pulse-width modulation scheme will be introduced for the newly developed configuration. The properties and functionality of the dual motor drive concept will be validated via several tests, which will be conducted using both a simulation program and a laboratory prototype.

II. DUAL TWO-LEVEL THREE-PHASE INVERTER VERSUS NINE-SWITCH INVERTER

In this section, it is presented a comparison of six-phase induction motor drive based on the dual two-level three-phase inverter and the alternative solution based on the nine-switch inverter with dual output, showing some advantages and disadvantages. In modern industrial electric vehicles, the most common solution for the traction system is given by a two-level inverter feeding a three-phase induction motor. The inverter is usually supplied by a bank of standard lead acid batteries or lately by a bank of lithium-ion batteries, often at very low voltage for safety reason. Due to this solution, it is quite difficult to create AC drives for high power ratings above 20 kW, due to the high cost of the resulting high-current semiconductor power switches of the inverter.

This problem limits the expansion of the AC drives for high power applications. Several solutions have been proposed in order to reduce the current rating of the power switches, such as the six-phase machine or dual three-phase machine supplied by a six-phase inverter. This solution allows to size the power switches at half of the rated current of an equivalent three-phase topology, but requires the realization of a six-phase machine and increases the control hardware and costs. A six-phase induction motor drive based on the dual two-level three-phase inverter can be seen in Fig.1 a). The solution is applied to an asymmetric ($\alpha = 30°$) six-phase motor with star winding connection. Six-phase induction motors with open windings allow different multilevel control strategies but require more power devices, such as the solution presented in Fig. 2.

Due to the high number of power devices for such applications, some topologies have been proposed in order to minimize their cost and size. This is the case of the AC drive based on the nine-switch inverter. A dual output nine-switch inverter applied to a six-phase phase induction motor with open windings can be seen in Fig. 1 b). Despite, the advantage of reducing the number of DC power sources and power semiconductors, and consequently the cost, volume and control complexity, it also introduces other disadvantages such as the fault-tolerant capability and limitations on the control range extension due to some unavailable voltage vectors as a consequence of less power devices. Several schemes regarding the dual two-level three-phase inverter applied to six-phase induction motors, dual motors or other types of motors, can be seen in [13], [41], [42], [43], [44], and [45]. In the case of the nine-switch inverter topologies, some important references can be used in [5], [6], [7], [40], [46], [47], and [48].

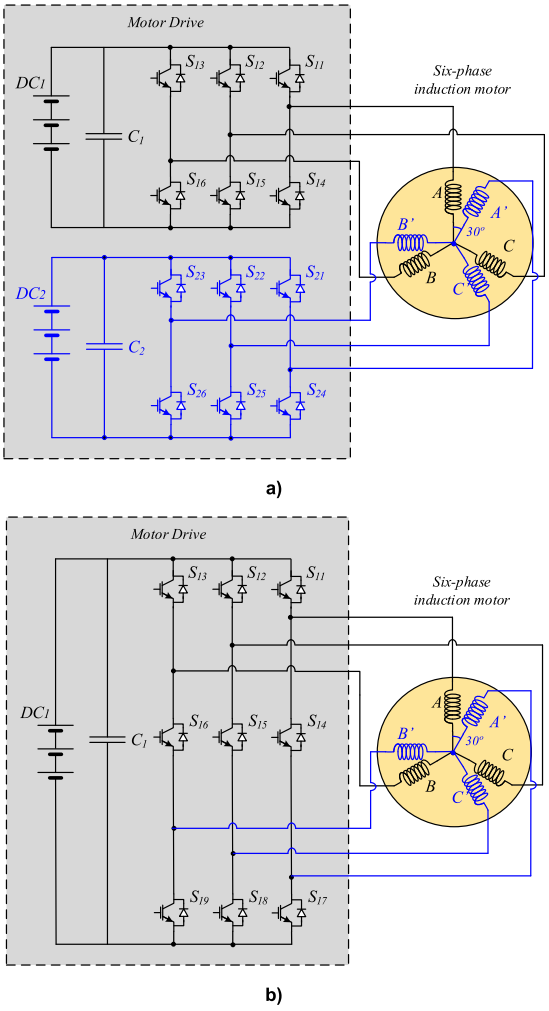

FIGURE 1. Classic dual output inverter topologies applied to an asymmetric six-phase induction motor: a) based on the dual two-level three-phase inverter and b) based on a nine-switch two-level inverter with dual output.

The next table present a comparison of the classic topologies presented in Fig. 1. This comparison can give to readers the perception of both advantages and disadvantages of such solutions. Nevertheless, this comparison cannot be generalized for all the topologies using similar structures and a detailed analysis should be done. Since this paper is dedicated to presenting a new multilevel topology, a comparison between similar topologies is presented in the following sections.

TABLE 1. Comparison of the classic topologies presented in Fig. 1.

	Fig 1 a)	Fig 1 b)
Number of power devices	12	9
Number of DC power sources	2	1
Number of capacitors	2	1
Number of voltage levels per phase	2	2
Max. voltage stress over power devices	V_{DC1} or V_{DC2}	V_{DC1}
Max. current stress over power devices (pu)	1	2
Control independence	Independent between inverters	Dependent as a single inverter
Control complexity	high	medium
Control range limitation	low	high
Fault tolerance capability	medium	low

The focus of this manuscript is only in the inverter stage, where the energy can become from a bank of batteries or another energy storage system, from any renewable energy source (RES) or even from the power grid. The energy flow can be bidirectional, depending on the control strategy and capability of the DC power sources, since some RES are not able to withstand bidirectional energy flow, such as solar photovoltaic systems. Despite not represented in Fig.2 or Fig.3, the DC bus circuit of the inverters can also be connected to rectifiers and supplied by the power grid. In this case, the capability to provide bidirectional energy flow depends on the controllability of the rectifier topology.

III. PROPOSED MULTILEVEL TOPOLOGY DERIVED FROM THE NINE-SWITCH INVERTER

Multilevel AC drives are a very well-known and successful solution used in industry due to the previously mentioned advantages. As mentioned before, there are many multilevel topologies. One of the modular topologies that uses classic

two-level three-phase voltage source inverters is the dual inverter. Although it uses two classical two-level inverters, it allows obtaining 9 voltage levels across each motor winding (considering both DC voltage sources are equal) [49], [50]. This topology, shown in Fig. 2 with its structure applied to a dual or six-phase motor drive, enables the generation of a significant number of voltage levels. Besides this characteristic, it also allows increasing the voltage applied to each winding. However, with the purpose to reduce the number of power semiconductor components, a new topology is proposed for a dual or six-phase motor AC drive, as shown in Fig. 3. Although the open winding configuration with a dual side supply is maintained, the number of legs for each of the sides is reduced from 6 to 3 legs. To achieve this reduction, the proposed topology uses legs with three switches.

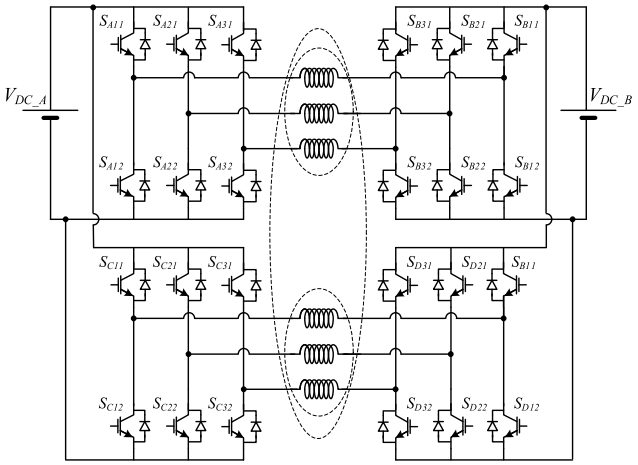

FIGURE 2. Classic multilevel dual-inverter topology for the six-phase or dual motor AC drive.

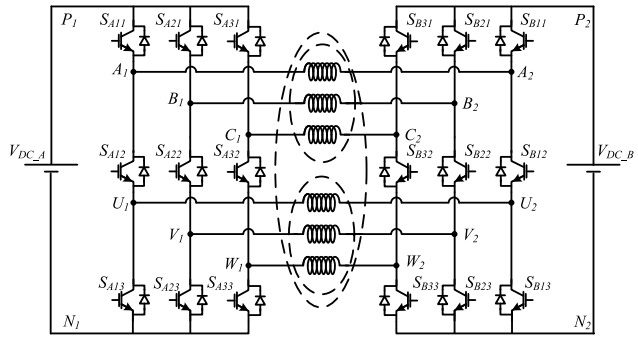

FIGURE 3. Proposed dual-inverter topology with reduced number of switches for the six-phase or dual motor AC drive.

To study the functionality of the suggested multilevel inverter and obtain the respective voltage and current relationships for each of the motors, a dynamic model is needed. The transistors and their associated antiparallel diodes are assumed to be ideal switches (zero *ON*-state voltages, zero *OFF*-state currents and negligible switching times). Therefore, each transistor/diode *ON* or *OFF* state can be represented by a binary variable, as follows:

$$\begin{cases} d_{Aij} = 1, & if\ S_{Aij}\ is\ ON \\ d_{Aij} = 0, & if\ S_{Aij}\ is\ OFF \\ d_{Bij} = 1, & if\ S_{Bwk}\ is\ ON \\ d_{Bij} = 0, & if\ S_{Bwk}\ is\ OFF \end{cases} \tag{1}$$

where $i = 1..3$ and $j = 1..3$

Upon examining each of the nine-switch inverters, excluding topological restrictions like open-circuits at the load terminals and short-circuits across the *DC* links, it becomes apparent that each leg can be seen as having only three possible operating modes, as illustrated in Fig. 4. As a result, in all possible combinations, it is ensured that for each leg, just two switches are in the *ON* state.

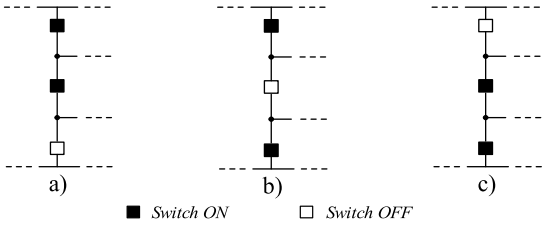

FIGURE 4. Possible operation modes for each leg of the proposed converter.

The pole voltages of the output terminals *A*, *B*, *C* and *U*, *V*, *W*, regarding the *N* terminal of each *DC* source, dependent on the possible switch state combination, are listed in Table 2. This table reveals that distinct winding voltages may be generated when connecting each leg to each side of the motor windings, even considering the physical constraint that imposes a pole voltage applied by the upper switches consistently higher than or equal to the voltage output in the lower switches side.

TABLE 2. Operation modes for the first leg.

Mode	Figure	Switches			Pole Voltages	
		S_{11}	S_{12}	S_{13}	v_{AN}	v_{UN}
PP	4 a)	1	1	0	V_{DC}	V_{DC}
PN	4 b)	1	0	1	V_{DC}	0
NN	4 c)	0	1	1	0	0

The pole voltages of each dual nine-switch inverter, at the output terminals *A*, *B*, *C* regarding the respective *N* terminal, denoted v_{h1}, v_{h2}, and at similar pole voltages of terminals *U*, *V*, *W*, denoted v_{l1}, v_{l2}, can be mathematically described in (2) as functions of the switches states (leg possible states are depicted in Fig. 4).

$$\begin{cases} v_{h1} = d_{Ai1}\ V_{DC\_A} \\ v_{l1} = d_{Ai1}\ d_{Ai2}\ V_{DC\_A} \\ v_{h2} = d_{Bi1}\ V_{DC\_B} \\ v_{l2} = d_{Bi1}\ d_{Bi2}\ V_{DC\_B} \end{cases} \tag{2}$$

where $h1 = A_1, B_1, C_1$, $l1 = U_1, V_1, W_1$, $h2 = A_2, B_2, C_2$ and $l2 = U_2, V_2, W_2$.

The voltages applied to each set of motor windings will be the combinations of the differences v_{h1}- v_{h2} for the upper windings and v_{l1}- v_{l2} for the lower ones. This provides several advantages for the *AC* drive. Firstly, it will extend the applied voltage to the windings. In effect, considering equal *DC* source voltages ($V_{DC\_A} = V_{DC\_B} = V_{DC}$), the maximum applied voltage will be 1.5 V_{DC} in each motor winding set, instead of the 2/3 V_{DC} when the drive was powered by just one nine-switch inverter. Secondly, it will allow multilevel winding voltages. In fact, with this proposed topology, considering equal *DC* source voltages (V_{DC}), it will be possible to obtain 19 voltage levels in each motor winding set. Fig. 5 illustrates the positive voltage levels during the positive half cycle for the motor winding $A_1\_A_2$. This visualization leads to the conclusion that the following 19 voltage levels, $-3/2\ V_{DC}$, $-4/3\ V_{DC}$, $-7/6\ V_{DC}$, $-1\ V_{DC}$, $-5/6\ V_{DC}$, $-2/3\ V_{DC}$, $-1/2\ V_{DC}$, $-1/3\ V_{DC}$, $-1/6\ V_{DC}$, 0, $+1/6\ V_{DC}$, $+1/3\ V_{DC}$, $+1/2\ V_{DC}$, $+2/3\ V_{DC}$, $+5/6\ V_{DC}$, $+1\ V_{DC}$, $+7/6\ V_{DC}$, $+4/3\ V_{DC}$, and $+3/2\ V_{DC}$ can be applied to each motor winding. The determination of the voltage levels applied to winding $A_1\_A_2$ can also be achieved through analysis of the corresponding equivalent circuit, which is derived based on the specific switch combination. Fig. 8 illustrates the corresponding equivalent circuits for each of the voltage levels presented in Fig. 7. So, for example, at the zero voltage level, it is possible to see (Fig. 8a) that we have a series connection of the parallel combination of two sets of three windings. Since the voltage sources have opposite polarities, the applied voltage is zero. The other equivalent circuits result in two loops with equivalent inductances that change according to the different parallels. Thus, by analyzing these circuits, it will be possible to obtain the 19 voltage levels for motor winding *A*.

To develop the dynamic model of the voltages applied to the two sets of motor windings by the two nine-switch inverters as a function of the switches combination, the superposition theorem is used. Therefore, the motor winding sets applied voltage will be given by the algebraic sum of the applied voltages by each nine-switch inverter. Considering the AC terminals of the inverters as a three-phase voltage system, their voltages regarding a virtual neutral point of those voltage sources (v_{O*}) will be given by eq. (3) and (4).

$$\begin{bmatrix} v_{A_1O} \\ v_{B_1O} \\ v_{C_1O} \\ v_{U_1O} \\ v_{V_1O} \\ v_{W_1O} \end{bmatrix} = \frac{1}{3} \begin{bmatrix} 2 & -1 & -1 & 0 & 0 & 0 \\ -1 & 2 & -1 & 0 & 0 & 0 \\ -1 & -1 & 2 & 0 & 0 & 0 \\ 0 & 0 & 0 & 2 & -1 & -1 \\ 0 & 0 & 0 & -1 & 2 & -1 \\ 0 & 0 & 0 & -1 & -1 & 2 \end{bmatrix} \begin{bmatrix} v_{A_1} \\ v_{B_1} \\ v_{C_1} \\ v_{U_1} \\ v_{V_1} \\ v_{W_1} \end{bmatrix} \tag{3}$$

$$\begin{bmatrix} v_{A_2O} \\ v_{B_2O} \\ v_{C_2O} \\ v_{U_2O} \\ v_{V_2O} \\ v_{W_2O} \end{bmatrix} = \frac{1}{3} \begin{bmatrix} 2 & -1 & -1 & 0 & 0 & 0 \\ -1 & 2 & -1 & 0 & 0 & 0 \\ -1 & -1 & 2 & 0 & 0 & 0 \\ 0 & 0 & 0 & 2 & -1 & -1 \\ 0 & 0 & 0 & -1 & 2 & -1 \\ 0 & 0 & 0 & -1 & -1 & 2 \end{bmatrix} \begin{bmatrix} v_{A_2} \\ v_{B_2} \\ v_{C_2} \\ v_{U_2} \\ v_{V_2} \\ v_{W_2} \end{bmatrix} \tag{4}$$

However, the voltages applied to the motor windings given by (3) and (4) do not consider the dependence between upper and lower legs. This dependence is due to the fact that there will be only one virtual neutral point (v_{O*}) being the inverter *AC* voltages, a function of the switching states. Thus, regarding the *AC* voltages of the upper and lower legs of the left nine-switch inverter, they will be given by (5) and (6), as shown at the bottom of the next page. As shown in these equations, there is an influence between the upper and lower *AC* terminals in the switching combination. The *AC* voltages of the right nine-switch inverter can easily be obtained from (5) and (6) since they are similar.

A further aspect to be considered in the determination of the winding voltages applied by each nine-switch inverter is the fact that the virtual neutral point of the motor windings (v_O^{**}) could be different from the virtual neutral point of the voltage sources (v_{O^*}). The voltage difference between these virtual points can be given by (7), as shown at the bottom of the next page.
where:

$$v_{O^*O^{**}} = \frac{1}{6}\left(v_{A_kO^{**}} + v_{B_kO^{**}} + v_{C_kO^{**}} + v_{U_kO^{**}} + v_{V_kO^{**}} + v_{W_kO^{**}}\right) \tag{8}$$

with $k = 1,2$,

Finally, the voltage applied to each motor winding will be determined by the contribution of the two nine-switch inverters, namely:

$$\begin{cases} v_{h1h2} = v_{h1O^{**}} - v_{h2O^{**}} \\ v_{l1l2} = v_{l1O^{**}} - v_{l2O^{**}} \end{cases} \tag{9}$$

Analysing the expressions of the motor windings applied voltages and assuming $V_{DC\_A} = V_{DC\_B} = V_{DC}$, it is possible to confirm the aforementioned 19 voltage levels in each motor winding set. It is also possible to verify that the maximum voltage applied to the motor windings is higher than the value of the *DC* voltage sources, namely 1.5 V_{DC}. Taking into account the number of possible operation modes for all the legs of the proposed two nine-switch multilevel inverter for open-end motors, it is concluded that this double nine-switch multilevel inverter presents 729 possible switch combinations. On the other hand, it is important to highlight a critical aspect commonly encountered in multilevel converters: the voltage balance between the upper and lower legs can be affected by the influence of switching states on the virtual neutral point. However, in the case of the proposed topology, both inverters are directly connected to voltage sources. As a result, the voltage sources maintain a fixed voltage value, ensuring that the virtual neutral point remains stable, even in scenarios involving asymmetrical loads or unequal current draw from the phases.

From the previous equations, it is also possible to derive the voltage vectors for the six-phase drive. Thus, the voltage vectors in the $\alpha\beta$ and xy reference frames, can be obtained using the amplitude-invariant Clarke transformation matrix

(equations 10 and 11).

$$[T_{six}] = \frac{1}{3}\begin{bmatrix} 1 & -1/2 & -1/2 & \sqrt{3}/2 & -\sqrt{3}/2 & 0 \\ 0 & \sqrt{3}/2 & -\sqrt{3}/2 & 1/2 & 1/2 & -1 \\ 1 & -1/2 & -1/2 & -\sqrt{3}/2 & \sqrt{3}/2 & 0 \\ 0 & -\sqrt{3}/2 & \sqrt{3}/2 & 1/2 & 1/2 & -1 \end{bmatrix} \tag{10}$$

$$\begin{bmatrix} v_\alpha & v_\beta & v_x & v_y \end{bmatrix} = [T_{six}] \begin{bmatrix} v_{A_1A_2} & v_{B_1B_2} & v_{C_1C_2} & v_{U_1U_2} & v_{V_1V_2} & v_{W_1W_2} \end{bmatrix} \tag{11}$$

The dual-inverter six-phase drive offers a significantly higher number of switching state combinations compared to the single-sided supply. Here, the two inverters can be controlled independently; therefore, in total, $64 \times 64 = 4096$ switching state combinations are available. This will result in 535 distinct voltage space vectors in the $\alpha\beta$ and xy planes, respectively, as illustrated in Fig. 7.

IV. MODULATION SCHEME

Regarding the suggested multilevel inverter, a modulation strategy can be devised based on a sinusoidal pulse-width modulation (*SPWM*) approach. However, existing *SPWM* modulator methods must be adapted to accommodate the multilevel modulation requirements, namely modulating waveforms for the upper and lower terminals of each nine-switch converter. Taking this into consideration, the normalized modulating signals for the upper *AC* terminals are expressed as follows:

$$\begin{cases} v_A = m_U \ \sin(\omega t + \phi_U) \\ v_B = m_U \ \sin\left(\omega t - \frac{2\pi}{3} + \phi_U\right) \\ v_C = m_U \ \sin\left(\omega t + \frac{2\pi}{3} + \phi_U\right) \end{cases} \tag{12}$$

Similarly, the normalized modulating signals for the lower *AC* terminals are given by:

$$\begin{cases} v_U = m_L \ \sin(\omega t + \phi_L) \\ v_V = m_L \ \sin(\omega t - \frac{2\pi}{3} + \phi_L) \\ v_W = m_L \ \sin(\omega t + \frac{2\pi}{3} + \phi_L) \end{cases} \tag{13}$$

where $\omega{=}2\pi f$, being f the fundamental frequency, φ_U and φ_L are the phase-shift angles, m_U and m_L are the modulation

$$\begin{cases} v_{A_1O^*} = (d_{A11}d_{A21}d_{A31})(1-d_{A13}d_{A23}d_{A33})\left(d_{A12}v_{U_1O} + (1-d_{A12})\left(1-\frac{d_{A21}d_{A22}d_{A31}d_{A32}}{2}\right)\left((d_{A21}d_{A22}v_{V_1O}) + (d_{A31}d_{A32}v_{W_1O})\right)\right) + (1-((d_{A11}d_{A21}d_{A31})(1-d_{A13}d_{A23}d_{A33})))\,v_{A_1O} + (d_{A11}d_{A21}d_{A31})(d_{A13}d_{A23}d_{A33})\frac{V_{DC\_A}}{2} \\ v_{B_1O^*} = (d_{A11}d_{A21}d_{A31})(1-d_{A13}d_{A23}d_{A33})\left(d_{A22}v_{V_1O} + (1-d_{A22})\left(1-\frac{d_{A11}d_{A12}d_{A31}d_{A32}}{2}\right)\left((d_{A11}d_{A12}v_{U_1O}) + (d_{A31}d_{A32}v_{W_1O})\right)\right) + (1-((d_{A11}d_{A21}d_{A31})(1-d_{A13}d_{A23}d_{A33})))\,v_{B_1O} + (d_{A11}d_{A21}d_{A31})(d_{A13}d_{A23}d_{A33})\frac{V_{DC\_A}}{2} \\ v_{C_1O^*} = (d_{A11}d_{A21}d_{A31})(1-d_{A13}d_{A23}d_{A33})\left(d_{A32}v_{W_1O} + (1-d_{A32})\left(1-\frac{d_{A11}d_{A12}d_{A21}d_{A22}}{2}\right)\left((d_{A11}d_{A12}v_{U_1O}) + (d_{A21}d_{A22}v_{V_1O})\right)\right) + (1-((d_{A11}d_{A21}d_{A31})(1-d_{A13}d_{A23}d_{A33})))\,v_{C_1O} + (d_{A11}d_{A21}d_{A31})(d_{A13}d_{A23}d_{A33})\frac{V_{DC\_A}}{2} \end{cases} \tag{5}$$

$$\begin{cases} v_{U_1O^*} = (1-d_{A11}d_{A21}d_{A31})(1-d_{A12}d_{A22}d_{A32})\left(d_{A12}v_{A_1O} + (1-d_{A12})\left(1-\frac{d_{A22}d_{A23}d_{A32}d_{A33}}{2}\right)\left((d_{A22}d_{A23}v_{B_1O}) + (d_{A32}d_{A33}v_{C_1O})\right)\right) + ((d_{A11}d_{A21}d_{A31}) + (d_{A12}d_{A22}d_{A32}))\,v_{U_1O} - (d_{A11}d_{A21}d_{A31})(d_{A13}d_{A23}d_{A33})\frac{V_{DC\_A}}{2} \\ v_{V_1O^*} = (1-d_{A11}d_{A21}d_{A31})(1-d_{A12}d_{A22}d_{A32})\left(d_{A22}v_{B_1O} + (1-d_{A22})\left(1-\frac{d_{A12}d_{A13}d_{A32}d_{A33}}{2}\right)\left((d_{A12}d_{A13}v_{A_1O}) + (d_{A32}d_{A33}v_{C_1O})\right)\right) + ((d_{A11}d_{A21}d_{A31}) + (d_{A12}d_{A22}d_{A32}))\,v_{V_1O} - (d_{A11}d_{A21}d_{A31})(d_{A13}d_{A23}d_{A33})\frac{V_{DC\_A}}{2} \\ v_{W_1O^*} = (1-d_{A11}d_{A21}d_{A31})(1-d_{A12}d_{A22}d_{A32})\left(d_{A32}v_{C_1O} + (1-d_{A32})\left(1-\frac{d_{A12}d_{A13}d_{A22}d_{A23}}{2}\right)\left((d_{A12}d_{A13}v_{A_1O}) + (d_{A22}d_{A23}v_{B_1O})\right)\right) + ((d_{A11}d_{A21}d_{A31}) + (d_{A12}d_{A22}d_{A32}))\,v_{W_1O} - (d_{A11}d_{A21}d_{A31})(d_{A13}d_{A23}d_{A33})\frac{V_{DC\_A}}{2} \end{cases} \tag{6}$$

$$\begin{cases} v_{h1O^{**}} = v_{h1O^*} + v_{O^*O^{**}} \\ v_{l1O^{**}} = v_{l1O^*} + v_{O^*O^{**}} \\ v_{h2O^{**}} = v_{h2O^*} + v_{O^*O^{**}} \\ v_{l2O^{**}} = v_{l2O^*} + v_{O^*O^{**}} \end{cases} \tag{7}$$

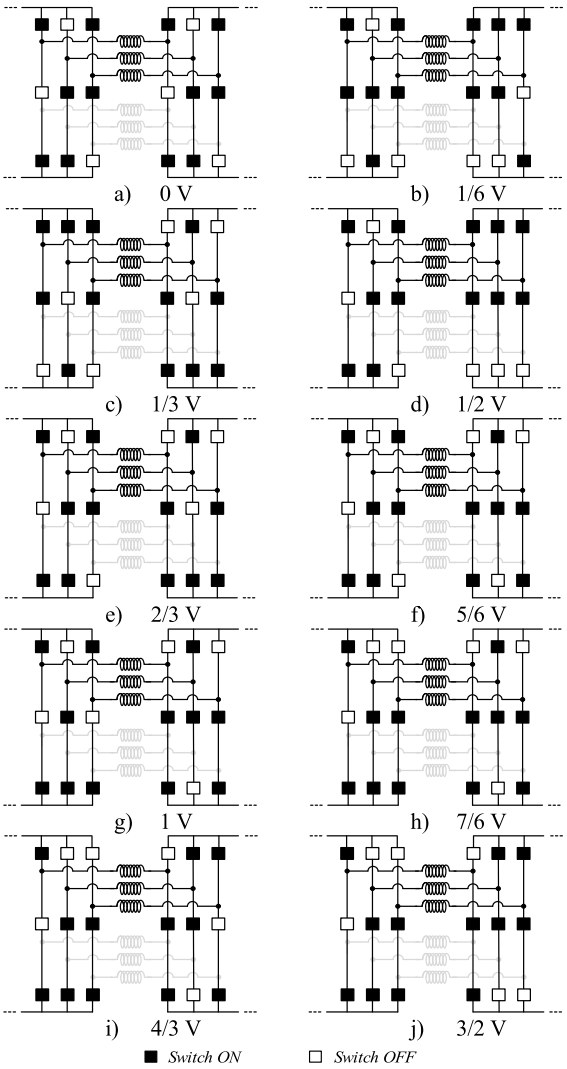

FIGURE 5. Example of the different voltage levels applied to the motor winding $A_1\_A_2$ for the positive half cycle.

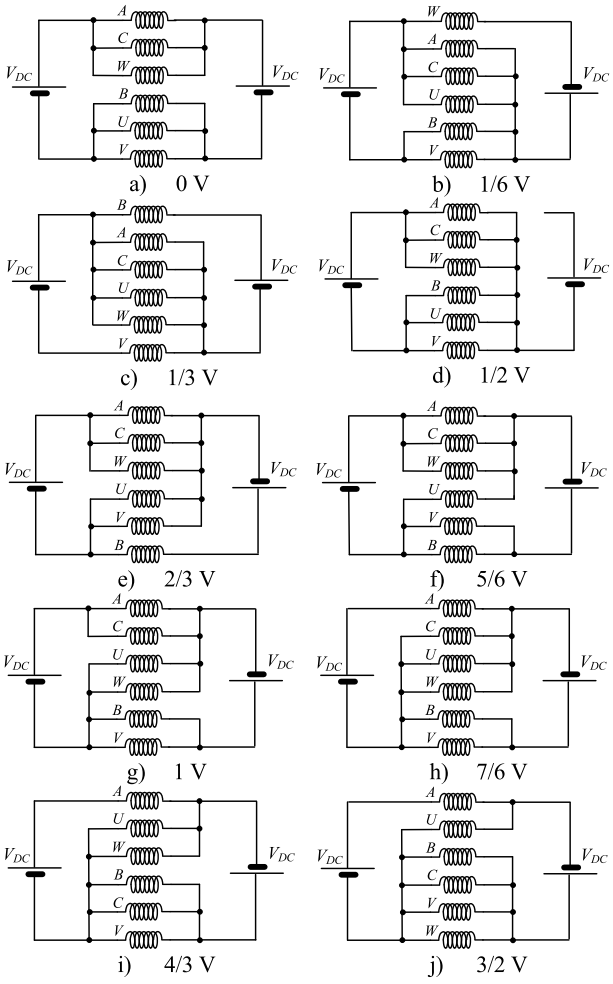

FIGURE 6. Equivalent circuits obtained from the different voltage levels applied to the motor winding $A_1\_A_2$ for the positive half cycle (see Fig. 5).

indexes with the linear range between 0 and 1. From the analysis of (12) and (13), it turns out that it is necessary to *DC* shift the modulating signals associated to the upper and lower *AC* terminals, so that they are far apart in the linear modulation range. In this way, it is necessary to add offsets (V_{offset}) in the modulating signals given by (12) and (13). Hence, the offset modulating signals will be given by:

$$\begin{cases} v_A = m_U \ \sin(\omega t + \phi_U) + V_{Uoffset} \\ v_B = m_U \ \sin\left(\omega t - \frac{2\pi}{3} + \phi_U\right) + V_{Uoffset} \\ v_C = m_U \ \sin\left(\omega t + \frac{2\pi}{3} + \phi_U\right) + V_{Uoffset} \end{cases} \tag{14}$$

and:

$$\begin{cases} v_U = m_L \ \sin(\omega t + \phi_L) + V_{Loffset} \\ v_V = m_L \ \sin\left(\omega t - \frac{2\pi}{3} + \phi_L\right) + V_{Loffset} \\ v_W = m_L \ \sin\left(\omega t + \frac{2\pi}{3} + \phi_L\right) + V_{Loffset} \end{cases} \tag{15}$$

where $V_{Uoffset} = (1\text{-}m_U)$ and $V_{Loffset} = (m_L\text{-}1)$

Using these modulating signals, the voltages of the inverter upper and lower terminals will contain the required fundamental components.

To generate the gating signals of the inverter *A* switches, the modulating signals given by (14) and (15) should be compared with a high frequency carrier. Regarding the nine-switch inverter *B* switches (inverter in the right part of Fig. 3), the modulating sinusoidal functions given by (14) and (15) shifted by one half period must be used. Additionally, the high frequency carrier should be shifted by one quarter of the high frequency period. The modulation strategy and the gate signals applied to the *A* legs of the two nine-switch converters are presented in Fig. 8.

The schematic circuits for the generation of the transistor gate signals considering the first leg of each nine-switch converter can be seen in Fig. 9. For the middle switch S_{A12}, the state of all other switches needs to be considered. Thus, the S_{A12} switch state is the logic *XOR* of the upper and lower signal switches (S_{A11} and S_{A13}) of the same leg.

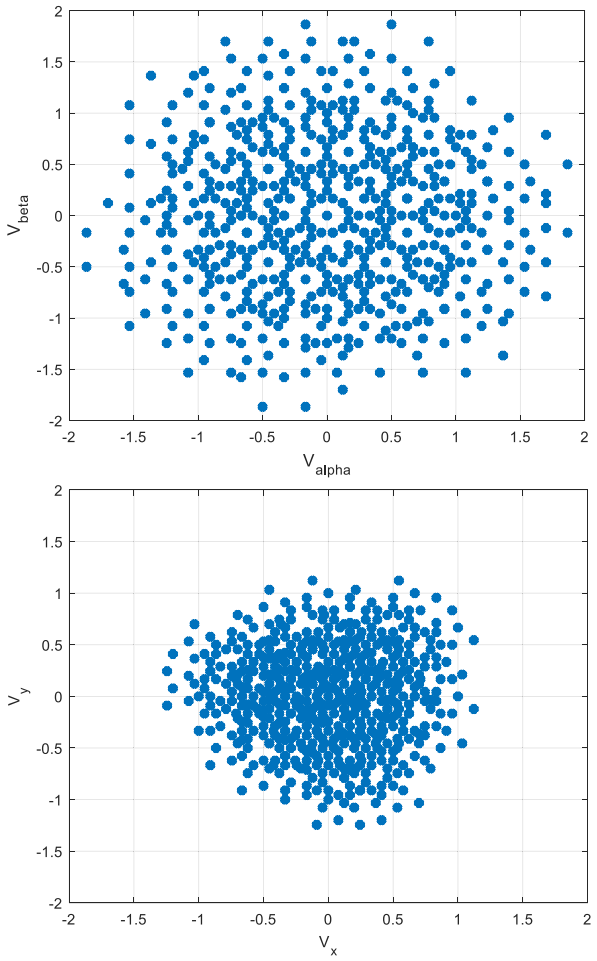

FIGURE 7. Voltage space vectors in the $\alpha\beta$ and xy planes for the six-phase drive.

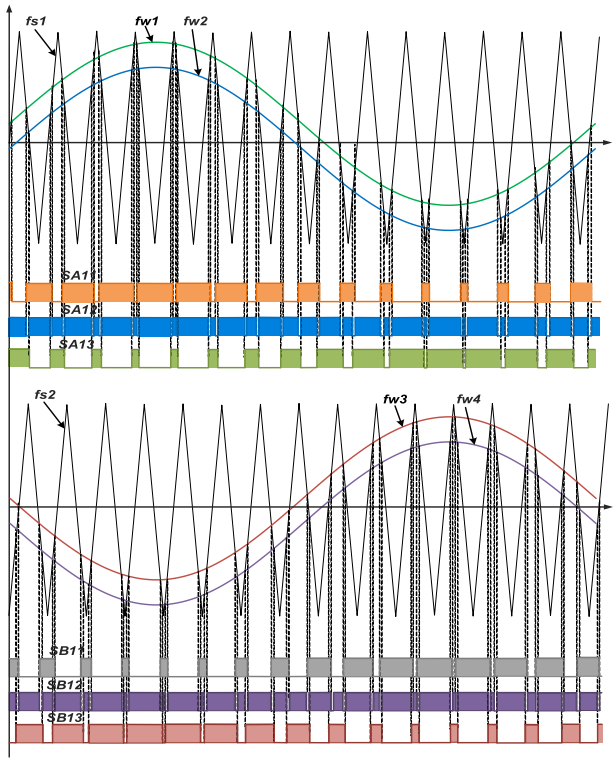

FIGURE 8. Modulation strategy and gating signals associated to the first leg of each nine-switch converter.

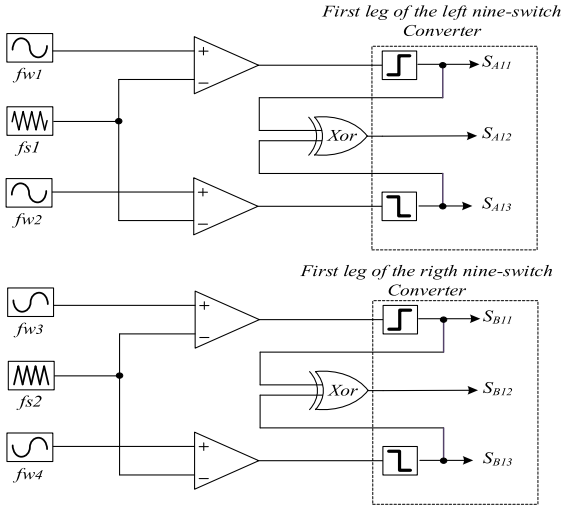

FIGURE 9. Schematic circuits for the generation of the transistor gate signals considering the first leg of each nine-switch converter.

As shown by the schematic circuits, this topology can still be operated in a way that is not very complex, since it is possible to implement a modulator like the SPWM.

To mention that multi-phase motors (such as six-phase IM) offer typically several advantages, such as reduced torque ripple, improved fault tolerance and lower harmonic content in the generated electromagnetic torque. This modulation strategy allows for the implementation of an open-loop voltage/frequency (v/f) control technique for six-phase induction motors powered by this multiphase multilevel inverter. Thus, this provides a straightforward way to control such motors, which is sufficient for some applications. However, there are some applications that require other closed-loop control. Thus, for this type of multi-phase motor and control drive in closed-loop control, even when certain limitations of these motors, such as harmonic content, must be mitigated, it becomes easier to analyze and control the machine's behavior by isolating the components in each subspace. In this way, other approaches, such as Variable Space Decomposition (VSD) transformation, can be used to simplify the analysis and control of six-phase machines by splitting the six-phase variables (e.g., currents and voltages) into orthogonal subspaces. These include the $\alpha\beta$-subspace, which shows the fundamental torque-producing components, the xy-subspace, which represents the non-torque-producing components associated with harmonics, and for higher phase-count motors, an additional z-subspace representing higher-order harmonic components.

TABLE 3. Comparison between multilevel topologies based on similar structures for dual or six-phase motors.

Topology	[31]	[32]	[33]	[34]	[35]	[36]	[37]	[38]	[39]	[40]	[41]	Proposed
Number of switches	24	48	36	84	18	36	20	21	18	21	20	18
Number of extra diodes	-	-	-	-	-	-	12	-				
Number of capacitors	-	12	2	23	-	8	2	2	2	2	2	-
Number of DC voltage sources	3	1	1	1	3	4	1	1	1	1	1	2
Number of voltage levels to each motor winding	9	17	9	13	3	11	9	9	9	9	9	19
Maximum voltage applied to each motor winding	$1.33V_{DC}$	$0.66V_{DC}$	$0.66V_{DC}$	V_{DC}	V_{DC}	$1.33V_{DC}$	$0.66V_{DC}$	$0.66V_{DC}$	$0.66V_{DC}$	$0.66V_{DC}$	$0.66V_{DC}$	$1.5\ V_{DC}$
All switches must withstand the same blocking voltage	yes	no	yes	no	yes	no	yes	no	yes	no	no	yes
Total Blocking Voltage (pu)	24	15.66	18	32	18	30	12.5	12.5	12.5	12	12.5	12.5
Scaled for motors requiring higher voltage	no	yes	yes	yes	no	no	yes	yes	no	no	no	no

V. COMPARISON ANALYSIS

A comparison of the characteristics of the suggested topology with other ones that have been given for multilevel topologies for the dual three-phase or six-phase motor drive system based on similar structures, is presented in Table 3. From this comparative table, it is possible to see that, the proposed and [35] topology are the ones that need fewer power semiconductors and passive components. However, topology [35] requires more DC power supplies, presents lower voltage levels and apply a lower maximum voltage applied to each motor winding. Another particular aspect that is possible to see is that, compared with some topologies, it does not require voltage divider capacitors nor a system to control the balance of its voltages. Another relevant aspect taken from this comparative table is that the proposed topology presents an important improvement is the number of voltage levels. In fact, it allows for obtaining a much higher number of voltage levels, 19, when compared with the maximum of 13 obtained by one of the other solutions (the other ones present fewer voltage levels). Another positive aspect is that the proposed topology is characterized by a higher maximum voltage level that can be applied to the motor winding. This allows for an expanded voltage range applied to the motor windings or a reduction in voltage stress across the switches. Another advantageous aspect of the proposed topology, but also of [31], [33], [35], [37], and [39] topologies is that all the switches must withstand the same blocking voltages. An analysis of the Total Blocking Voltage is also presented in the comparative table. The results indicate that the proposed topology ranks among those with the lowest values. Another aspect that is analyzed is the scalability of the converter for motors requiring higher voltage or power ratings. The proposed solution, as well as those presented in [31] and [35], lack the flexibility to incorporate module extensions, which is necessary for scaling the converters. Indeed, this is a limitation of the solution compared to other modular solutions. However, it is important to note that, compared to the classical two-level solution, the proposed approach enables its application to motors requiring higher voltages. This is because the proposed solution allows for an increase in the maximum applied voltage from 2/3 V_{DC} to 1.5 V_{DC}.

VI. SIMULATION RESULTS

The proposed multilevel converter for a dual-motor drive was firstly tested through several computer simulations. These tests were done using the well-known Matlab/Simulink. The main parameters of the simulated system included two 200 V *DC* voltage sources and a carrier frequency of 5 kHz.

Initially, both motors were driven with the fundamental frequency of 50 Hz and a modulation index (*MI*) of $m_U = m_L = 0.8$. The obtained waveforms for the voltages between the upper and lower *AC* terminals (first *A* leg) of the drive and the negative terminal of the *DC* voltage source are shown in Fig. 10. These results confirm the multilevel operation of the inverter, showing three levels. Regarding the voltages applied to the upper and lower motor windings (V_{A1A2}, V_{U1U2}), they are presented in Fig. 11 a) and b). It is seen that the obtained waveforms are very similar, being the multilevel operation confirmed. It is possible to distinguish the nineteen voltage levels. Regarding the Total Harmonic Distortion (*THD*) of the 19-level voltages a value of 29.7% was found, given the high amplitude of switching harmonics. It is also confirmed that the maximum peak voltage applied to the motor windings (300 V) is higher than the value of the *DC* voltage sources (200 V). The three-phase currents of the upper and bottom motor windings are presented in Fig. 12 a) and b), the currents being practically identical in both upper and bottom windings. The *THD* of the currents is much reduced, compared to the voltage *THD*, presenting a value of 1.26 %. Another aspect that was considered was a comparison with the conventional two-level topology (Fig. 1). In this way,

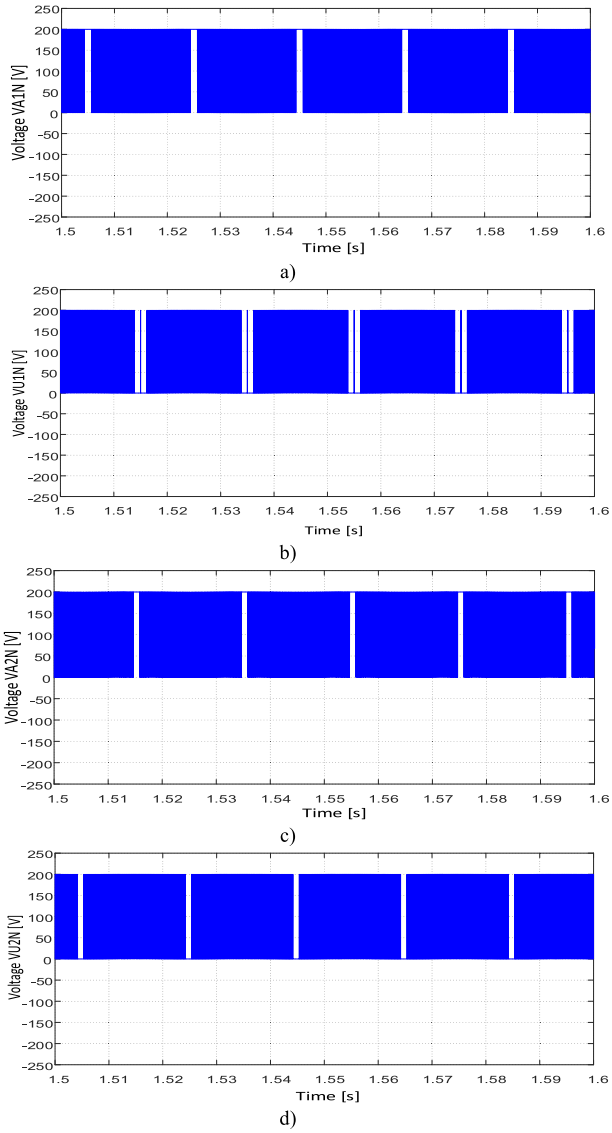

FIGURE 10. Waveforms of the voltages between the AC terminals of the inverter and the negative terminal of the DC voltage sources (first leg) obtained by simulation: a) Voltage over A_1-N_1; b) Voltage over A_2-N_2; c) Voltage over U_1-N_1; d) Voltage over U_2-N_2.

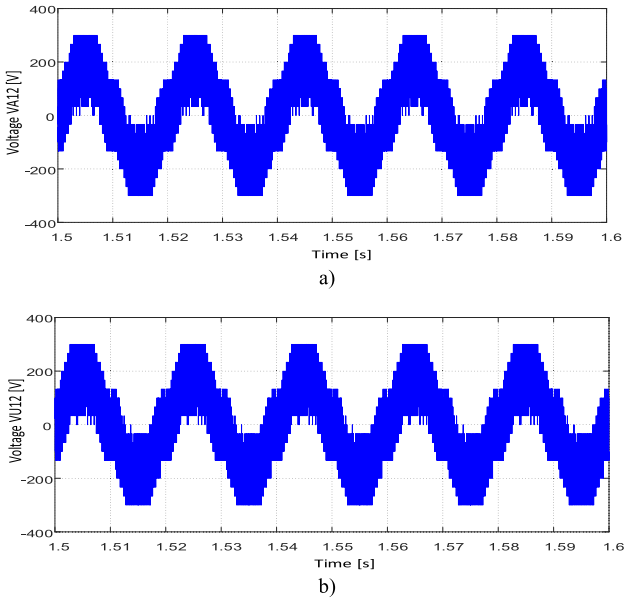

FIGURE 11. Waveforms of the voltages applied to the windings of the upper and lower motors obtained by simulation: a) VA1A2 b) VU1U2.

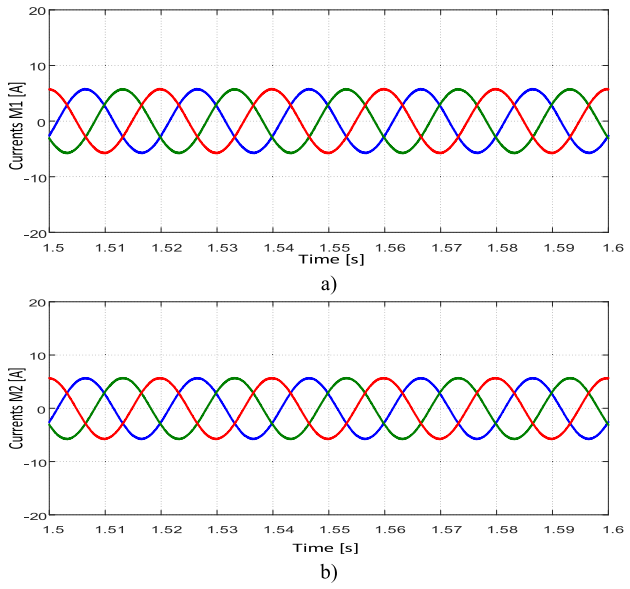

FIGURE 12. Waveforms of the three-phase currents of the motors obtained by simulation: a) upper motor b) bottom motor.

the conventional topology was also tested under the same conditions. This test resulted in a voltage THD of 72.4%. This clearly demonstrates that the increased number of voltage levels in the proposed solution significantly reduces the voltage THD (from 72.4% to 29.7%).

For a test in transient conditions, the drive was initially operated at 50 Hz and with a *MI* of $m_U = m_L = 0.8$. Afterwards at t = 1.6 s, the drive imposed a sudden change both in the frequency to 35 Hz and in the *MI* to $m_U = m_L = 0.6$. Fig. 13 shows the winding voltages. It is seen that the upper and lower motor winding voltage waveforms share similar patterns. Therefore, the three-phase currents of both upper and lower motor windings, presented in Fig. 14, are also very similar. This similarity is maintained after the transient due to the change of the modulating signal and *MI*.

VII. LABORATORY PROTOTYPE RESULTS

A prototype version of the proposed dual nine-switch inverter was built for practical tests in a laboratory environment. For comparison purposes, the prototype was built using the same parameters of the simulations and subjected to the same simulation tests already presented in section V. Fig. 15 shows a photography of the experimental setup of the proposed solution. In this picture it is possible see: 1 – Main DC power

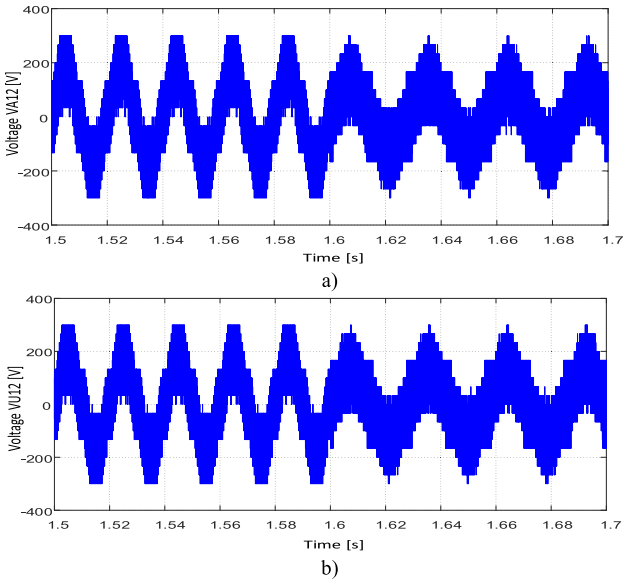

FIGURE 13. Waveforms of the voltages applied to the windings of the upper and lower motors with a sudden change of the modulating signal frequency and MI obtained by simulation: a) VA1A2 b) VU1U2.

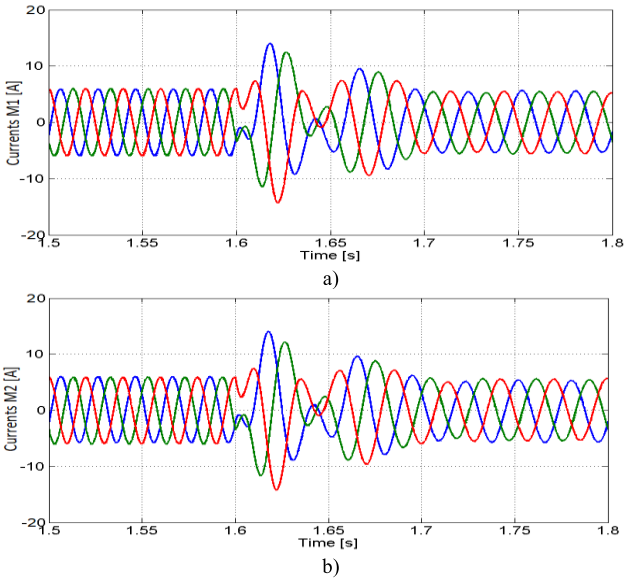

FIGURE 14. Waveforms of the three-phase currents of the motors with a sudden change of the modulating signal frequency and MI obtained by simulation: a) upper motor b) bottom motor.

sources (2 independent power sources); 2 – Oscilloscope; 3 – Digital Signal Processor DSPACE DS1104 Controller Board to generate the modulation scheme; 4 – Isolated gate drive circuit boards; 5 – Auxiliary DC power source for the isolated gate drive circuits; 6 – Dual Two-Level Nine-Switch Converter (2 independent power circuits) using individual modules Semikron SK 120 GAL 12F4 T (1200V, 120A) power IGBTs; 7 – Two open-winding induction motors; 8 – Mechanical loads imposed by coupled DC motors; 9 – Current probes for oscilloscope.

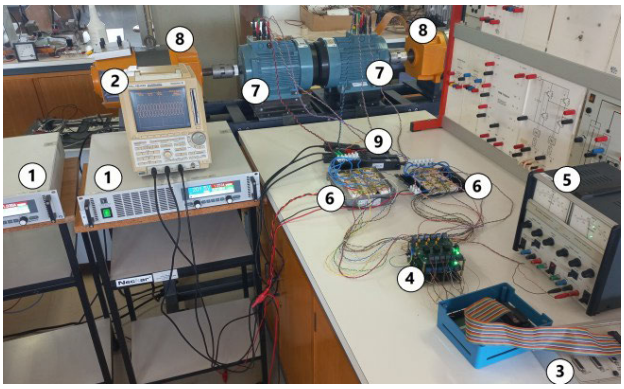

FIGURE 15. Photography of the experimental setup in the workbench. Devices identified in the text previous to this figure.

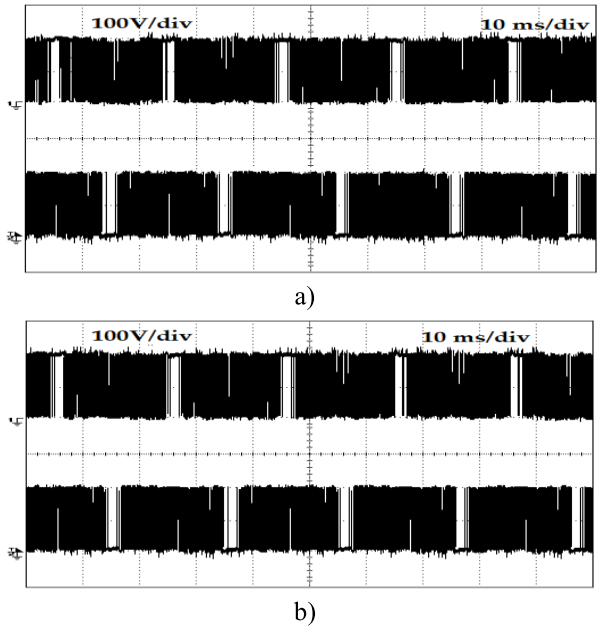

FIGURE 16. Waveforms of the voltages between the AC terminals of the inverter and the negative terminal of the DC voltage sources (first leg) obtained in laboratory: a) voltage over A_1-N_1 (Ch1) and A_2-N_2 (Ch2); b) voltage over U_1-N_1 (Ch1) and U_2-N_2 (Ch2).

The first laboratory test was done using the fundamental frequency of 50 Hz and a *MI* of $m_U = m_L = 0.8$. As shown in Fig. 16, the obtained waveforms for the voltages between the upper and lower *AC* terminals (first *A* leg) and the negative terminal of the *DC* voltage sources are similar to those obtained in simulation (Fig. 8). The same applies to waveforms of voltages at the upper and lower motor windings (V_{A1A2}, V_{U1U2}), which can be seen in Fig. 17. The *THD* of V_{A1A2} and V_{U1U2} voltages is of 32.3%, only slightly higher than the simulation results. The obtained waveforms of the three-phase currents, presented in Fig. 18, also confirm low distortion, presenting values of 2.92%.

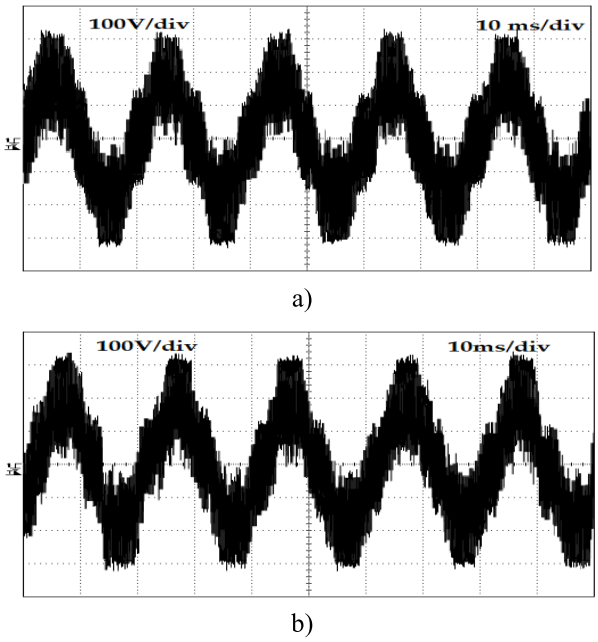

FIGURE 17. Waveforms of the voltages applied to the windings of the upper and lower motors obtained in laboratory: a) V_{AB} b) V_{UV}.

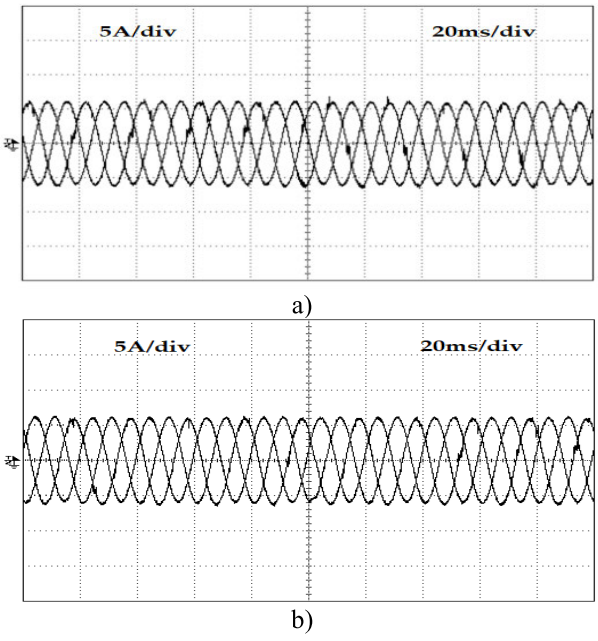

FIGURE 18. Waveforms of the three-phase currents of the motors at 50Hz obtained in laboratory: a) upper motor b) bottom motor.

Laboratory tests in transient conditions, similar to the transient simulation, were also made. The converter initially was operated with a modulating signal of 50 Hz and with a modulation index of $m_U = m_L = 0.8$, conditions that were suddenly changed to a frequency of 35 Hz and modulation index $m_U = m_L = 0.6$. The obtained results, presented in Figs. 19 and 20, show that the obtained waveforms are comparable to the ones obtained by simulation in Fig. 14.

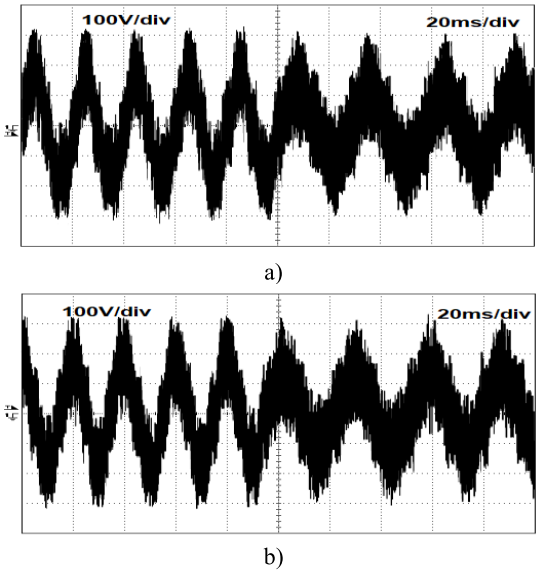

FIGURE 19. Waveforms of the voltages applied to the windings of the upper and lower motors with a sudden change of the modulating signal frequency and MI obtained in laboratory: a) V_{AB} b) V_{UV}.

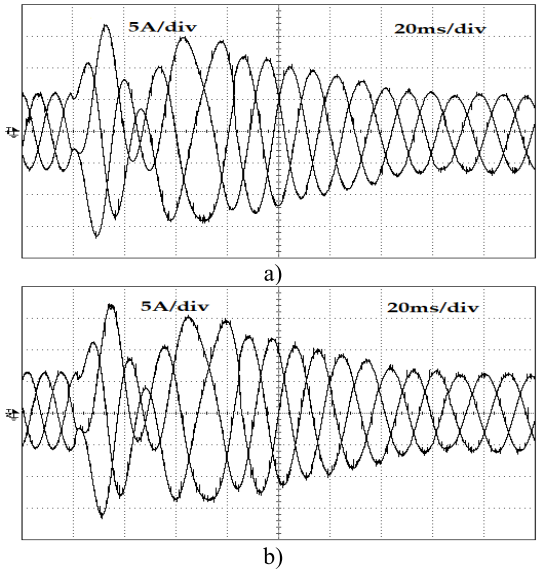

FIGURE 20. Waveforms of the three-phase currents of the motors with a sudden change of the modulating signal frequency and MI obtained in laboratory: a) upper motor b) bottom motor.

VIII. CONCLUSION

A multilevel converter derived from the nine-switch inverter for three-phase dual output applications, such as dual three-phase or six-phase motor drive system, was proposed in this article. The multilevel converter is modular and maintains the concept of reduced number of switches. It is characterized by the use of two nine-switch inverters in a dual inverter configuration. The proposed multilevel converter is characterized by a high number of voltage levels, as well as a comparatively small number of power semiconductors as inherited from the nine-switch inverter. Associated to the proposed topology, a *PWM* modulation was also presented to allow the operation of the proposed dual nine-switch

multilevel inverter as a sinusoidal *PWM* (*SPWM*) driven converter. The verification of the operation of the dual nine-switch multilevel inverter as well as its characteristics was made using computer simulations in Matlab/Simulink and a laboratory prototype. Both computer simulations and the laboratory prototype showed the multilevel waveforms and the number of levels. The high number of voltage levels and the dual motor drives allowed very low current *THDs* (1.26%-2.92%), which is a significant advantage taking into consideration the number of power switches.

REFERENCES

[1] F. Blaabjerg, S. Freysson, H.-H. Hansen, and S. Hansen, "A new optimized space-vector modulation strategy for a component-minimized voltage source inverter," *IEEE Trans. Power Electron.*, vol. 12, no. 4, pp. 704–714, Jul. 1997.

[2] R. Wang, J. Zhao, and Y. Liu, "A comprehensive investigation of four-switch three-phase voltage source inverter based on double Fourier integral analysis," *IEEE Trans. Power Electron.*, vol. 26, no. 10, pp. 2774–2787, Oct. 2011.

[3] C.-S. Lim, E. Levi, M. Jones, N. A. Rahim, and W.-P. Hew, "A comparative study of synchronous current control schemes based on FCS-MPC and PI-PWM for a two-motor three-phase drive," *IEEE Trans. Ind. Electron.*, vol. 61, no. 8, pp. 3867–3878, Aug. 2014.

[4] Y. Hu, S. Huang, X. Wu, and X. Li, "Control of dual three-phase permanent magnet synchronous machine based on five-leg inverter," *IEEE Trans. Power Electron.*, vol. 34, no. 11, pp. 11071–11079, Nov. 2019.

[5] T. Kominami and Y. Fujimoto, "A novel nine-switch inverter for independent control of two three-phase loads," in *Proc. IEEE Ind. Appl. Annu. Meeting*, Sep. 2007, pp. 2346–2350.

[6] M. K. Pinjala and R. Bhimasingu, "Improving the DC-link utilization of nine-switch boost inverter suitable for six-phase induction motor," *IEEE Trans. Transport. Electrific.*, vol. 6, no. 3, pp. 1177–1187, Sep. 2020.

[7] O. Gulbudak and M. Gokdag, "Dual-hysteresis band control of nine-switch inverter to control two induction motors," *IEEE Trans. Energy Convers.*, vol. 37, no. 2, pp. 788–799, Jun. 2022.

[8] W. Taha, P. Azer, A. D. Callegaro, and A. Emadi, "Multiphase traction inverters: State-of-the-art review and future trends," *IEEE Access*, vol. 10, pp. 4580–4599, 2022.

[9] L. Franquelo, J. Rodriguez, J. Leon, S. Kouro, R. Portillo, and M. Prats, "The age of multilevel converters arrives," *IEEE Ind. Electron. Mag.*, vol. 2, no. 2, pp. 28–39, Jun. 2008.

[10] S. Kouro, M. Malinowski, K. Gopakumar, J. Pou, L. G. Franquelo, B. Wu, J. Rodriguez, M. A. Pérez, and J. I. Leon, "Recent advances and industrial applications of multilevel converters," *IEEE Trans. Ind. Electron.*, vol. 57, no. 8, pp. 2553–2580, Aug. 2010.

[11] H. Abu-Rub, J. Holtz, J. Rodriguez, and G. Baoming, "Medium-voltage multilevel convertes—State of the art, challenges, and requirements in industrial applications," *IEEE Trans. Ind. Electron.*, vol. 57, no. 8, pp. 2581–2596, Aug. 2010.

[12] V. Jayakumar, B. Chokkalingam, and J. L. Munda, "A comprehensive review on space vector modulation techniques for neutral point clamped multi-level inverters," *IEEE Access*, vol. 9, pp. 112104–112144, 2021.

[13] Z. Huang, T. Yang, P. Giangrande, M. Galea, and P. Wheeler, "Technical review of dual inverter topologies for more electric aircraft applications," *IEEE Trans. Transport. Electrific.*, vol. 8, no. 2, pp. 1966–1980, Jun. 2022.

[14] I. R. F. M. P. da Silva, C. B. Jacobina, A. C. Oliveira, G. A. de Almeida Carlos, and M. B. de Rossiter Corrêa, "Hybrid modular multilevel DSCC inverter for open-end winding induction motor drives," *IEEE Trans. Ind. Appl.*, vol. 53, no. 2, pp. 1232–1242, Mar. 2017.

[15] V. F. Pires, D. Foito, and J. F. Silva, "Fault-tolerant multilevel topology based on three-phase H-bridge inverters for open-end winding induction motor drives," *IEEE Trans. Energy Convers.*, vol. 32, no. 3, pp. 895–902, Sep. 2017.

[16] S. Pramanick, M. Boby, N. A. Azeez, K. Gopakumar, and S. S. Williamson, "A three-level dodecagonal space vector-based harmonic suppression scheme for open-end winding IM drives with single-DC supply," *IEEE Trans. Ind. Electron.*, vol. 63, no. 11, pp. 7226–7233, Nov. 2016, doi: 10.1109/TIE.2016.2538205.

[17] W. Taha, F. Juarez-Leon, M. Hefny, A. Jinesh, M. Poulton, B. Bilgin, and A. Emadi, "Holistic design and development of a 100 kW SiC-based six-phase traction inverter for an electric vehicle application," *IEEE Trans. Transport. Electrific.*, vol. 10, no. 2, pp. 4616–4627, Sep. 2023.

[18] C. T. P. Nguyen, B.-H. Nguyên, J. P. F. Trovão, and M. C. Ta, "Torque distribution optimization for a dual-motor electric vehicle using adaptive network-based fuzzy inference system," *IEEE Trans. Energy Convers.*, vol. 38, no. 4, pp. 2784–2795, Dec. 2023, doi: 10.1109/TEC.2023.3285225.

[19] U. R. Muduli, A. R. Beig, K. A. Jaafari, K. A. Hosani, A. S. Al-Sumaiti, and R. K. Behera, "Dual motor power sharing control for electric vehicles with battery power management," *IEEE Trans. Ind. Electron.*, vol. 70, no. 12, pp. 12024–12035, Dec. 2023, doi: 10.1109/TIE.2023.3236096.

[20] C. Zhu, Q. Tu, C. Jiang, M. Pan, and H. Huang, "A cross coupling control strategy for dual-motor speed synchronous system based on second order global fast terminal sliding mode control," *IEEE Access*, vol. 8, pp. 217967–217976, 2020.

[21] P. P. Das, S. Satpathy, and S. Bhattacharya, "A six-phase space vector PWM technique for wide bandgap device-based three-level inverters," *IEEE Trans. Transport. Electrific.*, vol. 10, no. 3, pp. 5819–5830, Sep. 2024, doi: 10.1109/tte.2023.3319271.

[22] I. Lopez, S. Ceballos, J. Pou, J. Zaragoza, J. Andreu, I. Kortabarria, and V. G. Agelidis, "Modulation strategy for multiphase neutral-point-clamped converters," *IEEE Trans. Power Electron.*, vol. 31, no. 2, pp. 928–941, Feb. 2016.

[23] E. A. R. E. Ariff, O. Dordevic, and M. Jones, "A space vector PWM technique for a three-level symmetrical six-phase drive," *IEEE Trans. Ind. Electron.*, vol. 64, no. 11, pp. 8396–8405, Nov. 2017.

[24] V. Jayakumar, B. Chokkalingam, and J. L. Munda, "A twenty five switch inverter topology for controlling two independent five-phase load," *IEEE Access*, vol. 10, pp. 81722–81740, 2022.

[25] S. Tedeschini, S. Mohamadian, and C. Cecati, "A multi-phase multilevel powertrain for full electric aircraft," in *Proc. 47th Annu. Conf. IEEE Ind. Electron. Soc. (IECON)*, Oct. 2021, pp. 1–6.

[26] R. V. Nair, R. Chattopadhyay, S. Parashar, S. Bhattacharya, and K. Gopakumarb, "Cascaded active neutral point clamped and flying capacitor inverter topology for induction motor drives applications," in *Proc. IEEE Energy Convers. Congr. Exposit.*, Sep. 2018, pp. 6696–6702.

[27] M. I. Daoud, A. A. Elserougi, A. M. Massoud, R. Bojoi, A. S. Abdel-Khalik, and S. Ahmed, "Zero-/low-speed operation of multiphase drive systems with modular multilevel converters," *IEEE Access*, vol. 7, pp. 14353–14365, 2019.

[28] J. Wen and K. M. Smedley, "Hexagram inverter for medium-voltage six-phase variable-speed drives," *IEEE Trans. Ind. Electron.*, vol. 55, no. 6, pp. 2473–2481, Jun. 2008.

[29] A. C. N. Maia, C. B. Jacobina, N. B. de Freitas, and I. R. F. M. P. da Silva, "Open-end multilevel six-phase machine drive system with five three-leg converters," *IEEE Trans. Ind. Appl.*, vol. 53, no. 3, pp. 2271–2281, May 2017.

[30] G. Grandi, A. Tani, P. Sanjeevikumar, and D. Ostojic, "Multi-phase multi-level AC motor drive based on four three-phase two-level inverters," in *Proc. Int. Symp. Power Electron., Electr. Drives, Autom. Motion*, Jun. 2010, pp. 1768–1775.

[31] V. F. M. B. Melo, C. B. Jacobina, and N. Rocha, "Fault tolerance performance of dual-inverter-based six-phase drive system under single-, two-, and three-phase open-circuit fault operation," *IET Power Electron.*, vol. 11, no. 1, pp. 212–220, Jan. 2018.

[32] V. Nair, S. Pramanick, K. Gopakumar, and L. G. Franquelo, "Novel symmetric six-phase induction motor drive using stacked multilevel inverters with a single DC link and neutral point voltage balancing," *IEEE Trans. Ind. Electron.*, vol. 64, no. 4, pp. 2663–2670, Apr. 2017.

[33] P. P. Das, S. Satpathy, and S. Bhattacharya, "An online open-circuit fault diagnosis technique for three-level inverter-fed six-phase PMSM drives," *IEEE Trans. Power Electron.*, vol. 39, no. 11, pp. 14974–14987, Nov. 2024.

[34] A. K. Yadav, K. Gopakumar, R. K. Raj, L. Umanand, K. Matsuse, and H. Kubota, "Instantaneous balancing of neutral-point voltages for stacked DC-link capacitors of a multilevel inverter for dual-inverter-fed induction motor drives," *IEEE Trans. Power Electron.*, vol. 34, no. 3, pp. 2505–2514, Mar. 2019.

[35] E. L. Soares, C. B. Jacobina, N. B. de Freitas, N. Rocha, A. C. N. Maia, and A. M. N. Lima, "A multilevel open-end winding six-phase induction motor drive topology based on three two-level three-phase inverters," *IEEE Trans. Ind. Appl.*, vol. 59, no. 5, pp. 6360–6372, Oct. 2023.

[36] S. Padmanaban, F. Blaabjerg, P. W. Wheeler, P. Siano, L. Martirano, and P. Szczesniak, "A novel multilevel quad-inverter configuration for quasi six-phase open-winding converter," in *Proc. 10th Int. Conf. Compat., Power Electron. Power Eng. (CPE-POWERENG)*, Jun. 2016, pp. 325–330.
[37] R. Wang, L. Ai, and C. Liu, "A novel three-phase dual-output neutral-point-clamped three-level inverter," *IEEE Trans. Power Electron.*, vol. 36, no. 7, pp. 7576–7586, Jul. 2021.
[38] J. Monteiro, V. F. Pires, J. F. Silva, and S. Pinto, "A dual output NPC-type converter with a model predictive controller with compensation of DC capacitor voltage imbalance," in *Proc. 17th IEEE Int. Conf. Compat., Power Electron. Power Eng.*, Jun. 2023, pp. 1–6.
[39] R. Wang, S. Yuan, C. Liu, D. Guo, and X. Shao, "A three-phase dual-output T-Type three-level converter," *IEEE Trans. Power Electron.*, vol. 38, no. 2, pp. 1844–1859, Feb. 2023.
[40] A. Cordeiro, V. F. Pires, D. Foito, and J. F. Silva, "Six-phase fault-tolerant inverter using a multilevel nine-switch converter," in *Proc. IEEE 64th Int. Sci. Conf. Power Electr. Eng. Riga Tech. Univ. (RTUCON)*, Oct. 2023, pp. 1–8.
[41] C. I. Odeh, A. Lewicki, M. Morawiec, and J. O. Ojo, "A five-leg three-level dual-output inverter," *IEEE Trans. Circuits Syst. II, Exp. Briefs*, vol. 70, no. 2, pp. 690–694, Feb. 2023.
[42] V. F. Pires, J. Monteiro, A. Cordeiro, and J. F. Silva, "Integrated battery charger for electric vehicles based on a dual-inverter drive and a three-phase current rectifier," *Electronics*, vol. 8, no. 10, p. 1199, Oct. 2019.
[43] G. Grandi, C. Rossi, A. Lega, and D. Casadei, "Multilevel operation of a dual two-level inverter with power balancing capability," in *Proc. Conf. Rec. IEEE Ind. Appl. Conf. 41st IAS Annu. Meeting*, Tampa, FL, USA, Oct. 2006, pp. 603–610.
[44] Y. Kumsuwan and W. Srirattanawichaikul, "A space vector modulation strategy for three-level operation based on dual two-level voltage source inverters," in *Proc. Int. Power Electron. Conf. (IPEC-Hiroshima-ECCE ASIA)*, May 2014, pp. 3417–3424.
[45] S.-I. Hwang, J.-H. Jung, and J.-M. Kim, "Opposite triangle carrier method for common-mode voltage reduction in dual three-phase motor drive," in *Proc. IEEE 9th Int. Power Electron. Motion Control Conf. (IPEMC-ECCE Asia)*, Nov. 2020, pp. 346–351.
[46] Z. Shen, D. Jiang, Z. Liu, D. Ye, and J. Li, "Common-mode voltage elimination for dual two-level inverter-fed asymmetrical six-phase PMSM," *IEEE Trans. Power Electron.*, vol. 35, no. 4, pp. 3828–3840, Apr. 2020.
[47] M. S. Diab, A. A. Elserougi, A. S. Abdel-Khalik, A. M. Massoud, and S. Ahmed, "A nine-switch-converter-based integrated motor drive and battery charger system for EVs using symmetrical six-phase machines," *IEEE Trans. Ind. Electron.*, vol. 63, no. 9, pp. 5326–5335, Sep. 2016.
[48] Z. Qin, P. C. Loh, and F. Blaabjerg, "Application criteria for nine-switch power conversion systems with improved thermal performance," *IEEE Trans. Power Electron.*, vol. 30, no. 8, pp. 4608–4620, Aug. 2015.
[49] V. Pires, J. Martins, and H. Chen, "Dual-Inverter for grid-connected photovoltaic system: Modeling and sliding mode control," *Sol. Energy*, vol. 86, no. 7, pp. 2106–2115, Jul. 2012.
[50] G. Grandi, C. Rossi, D. Ostojic, and D. Casadei, "A new multilevel conversion structure for grid-connected PV applications," *IEEE Trans. Ind. Electron.*, vol. 56, no. 11, pp. 4416–4426, Nov. 2009.

V. FERNÃO PIRES (Senior Member, IEEE) received the B.S. degree in electrical engineering from the Institute Superior of Engineering of Lisbon, Portugal, in 1988, and the M.S. and Ph.D. degrees in electrical and computer engineering from the Technical University of Lisbon, Portugal, in 1995 and 2000, respectively.

Since 1991, he has been a member of the Teaching Staff with the Electrical Engineering Department, Superior Technical School of Setúbal—Polytechnic Institute of Setúbal. He is currently a Professor, teaching power electronics and control of power converters. He is also a Researcher with the Instituto de Engenharia de Sistemas e Computadores, Investigação e Desenvolvimento em Lisboa (INESC-ID). His work has resulted in more than 200 publications. His current research interests include the areas of power-electronic converters, fault diagnosis and fault tolerant operation, renewable energy, electrical vehicles, electrical drives, and power quality.

ARMANDO CORDEIRO (Member, IEEE) was born in Portugal, in 1976. He received the B.S. degree in electrical engineering from the Instituto Superior de Engenharia de Lisboa, in 1999, and the M.Sc. and Ph.D. degrees in electrical engineering from IST, Technical University of Lisbon, in 2004 and 2015, respectively. He has been a Professor with the Department of Electrical Engineering and Automation, Instituto Superior de Engenharia de Lisboa, for the area of automation, since 2006. His current research interests include the areas of power-electronic converters, industrial automation, and robotics. His research interests include power electronics, variable speed drives, automation systems, and electrical vehicles.

DANIEL FOITO received the Dipl.-Ing. and M.S. degrees in electrical engineering from the Instituto Superior Técnico, Technical University of Lisbon, Lisbon, Portugal, in 1993 and 2002, respectively, and the Ph.D. degree in electrical engineering from the Faculty of Sciences and Technology, New University of Lisbon, Portugal, in 2015. Since 1997, he has been a member of the Teaching Staff with the Electrical Engineering Department, Superior Technical School of Setúbal—Polytechnic Institute of Setúbal. He is currently an Adjoint Professor, teaching power electronics and electric drives. His research interests include renewable energy generation, electrical machines, electric drives, electric vehicle, fault diagnosis, and fault tolerant operation.

A. J. PIRES received the Graduate, M.Sc., and Ph.D. degrees in electrical engineering from the Instituto Superior Técnico (IST), Technical University of Lisbon, Lisbon, Portugal, in 1985, 1988, and 1994, respectively.

Currently, he is a Full Professor in the area of electrical engineering with the Polytechnic Institute of Setúbal, Setúbal, Portugal, and a Senior Researcher with the CTS-UNINOVA (Nova Lisbon University) and LASI, Portugal. His research interests include electrical machines, power electronics, intelligent control systems for electrical drives, and nonlinear systems.

J. FERNANDO A. SILVA (Life Senior Member, IEEE) was born in Monção Portugal, in 1956. He received the Dipl.-Ing. degree in electrical engineering and the Doctor degree in electrical and computer engineering (power electronics and control) from the Instituto Superior Técnico (IST), Universidade Técnica de Lisboa (UTL), Lisbon, Portugal, in 1980 and 1990, respectively. He is currently a Full Professor in power electronics and energy storage in the scientific area of energy with the Department of Electrical and Computer Engineering, Instituto Superior Técnico (IST), Universidade de Lisboa (UL). He is also a Senior Researcher with the Instituto de Engenharia de Sistemas e Computadores—Investigação e Desenvolvimento em Lisboa (INESC-ID). He is also an Associate Editor of IEEE TRANSACTIONS ON INDUSTRIAL ELECTRONICS, from 2000 to 2019, has been a member of the Editorial Board of *IEEE Industrial Electronics Magazine*, since 2010, and a member of Portuguese Engineering Society.

HAO CHEN (Senior Member, IEEE) received the B.S. and Ph.D. degrees in electrical engineering from the Department of Automatic Control, Nanjing University of Aeronautics and Astronautics, Nanjing, China, in 1991 and 1996, respectively.

He became an Associate Professor with the School of Information and Electrical Engineering, China University of Mining and Technology, Xuzhou, China, in 1998, where he has been a Professor, since 2001. From 2002 to 2003, he was a Visiting Professor with Kyungsung University, Busan, South Korea. Since 2008, he has also been an Adjunct Professor with the University of Western Australia, Perth, Australia. He is the author of one book and has also authored more than 190 articles. He is the holder of 14 U.S. patents, 23 Australian patents, one Danish patent, seven Canadian patents, three South African patents, ten Russian patents, 44 Chinese invention patents, and six Chinese utility model patents. His current research interests include motor control, linear launcher, electric vehicles, electric traction, servo drives, and wind power generator control.

Prof. Chen was a recipient of both the Prize of Science and Technology of Chinese Youth and the Prize of the Fok Ying Tong Education Foundation for Youth Teachers, in 2004. He received the First Prize in the Science and Technology Advanced of Province and Ministry once, the Second Prize in the Science and Technology Advanced of Province and Ministry seven times, and the Third Prize in the Science and Technology Advanced of Province and Ministry 14 times. He became the Chinese New Century Hundred-Thousand-Ten thousand Talents Engineering National Talent, in 2007, and won the Government Especial Allowance of People's Republic of China State Department, since 2006.